/
Article / Book Information

Title	A Soft Crawling Robot That Can Self-Repair Material Removal and Deep Lengthwise Cuts, Actuated by Thin McKibben Muscles
Authors	MENGFEI XIE, Yunhao Feng, Hiroyuki Nabae, Koichi Suzumori
Citation	IEEE Robotics and Automation Letters, Volume 9, Issue 6, pp. 5030-5037
Pub. date	2024, 4
DOI	https://doi.org/10.1109/LRA.2024.3386456
Creative Commons	Information is in the article.

A Soft Crawling Robot That Can Self-Repair Material Removal and Deep Lengthwise Cuts, Actuated by Thin McKibben Muscles

Mengfei Xie ⬝, Yunhao Feng ⬝, Hiroyuki Nabae ⬝, *Member, IEEE*, and Koichi Suzumori ⬝, *Senior Member, IEEE*

Abstract—Soft robots are prone to damage when they come into contact with sharp objects, decreasing their functionality. Self-repairing soft robots have great potential to restore their functionality after the damage has been repaired. However, for certain damages wherein it is difficult to reconnect the cut surfaces, the existing self-repairing soft robots often require external intervention to establish contact between the cut surfaces and achieve recovery. Therefore, this letter proposes a novel self-repairing soft robot composed of thin McKibben muscles and self-healing materials. Experimental validation and mathematical model analysis have demonstrated that this robot can self-repair the hard-to-reconnect cut surface damages, such as material removal and deep lengthwise cuts, by actuating the thin McKibben muscles in the designed sequence. Furthermore, experimental evidence through bending and crawling confirms that this robot exhibits robust self-repair properties. Moreover, this can be achieved without external intervention and shows potential to be extrapolated to other systems.

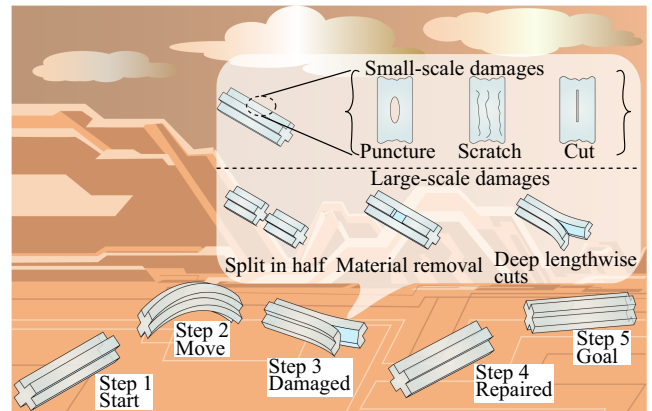*Index Terms*—Damage closure, McKibben muscle, self-repair, soft robot.

Fig. 1. Schematic of a self-repairing soft robot exploring unstructured environments. After suffering damage, the robot can autonomously fully repair itself and complete the exploration task. This paper discusses two types of damage modes: Material removal and deep lengthwise cuts.

I. INTRODUCTION

SOFT robots have high shape adaptability, which makes them suitable for use as manipulators [1], [2], [3] for grasping objects of different structures and as locomotion robots [4], [5], [6] in unstructured environments. However, a notable drawback is their vulnerability to sharp objects, which can affect their practical application. A promising approach to address this vulnerability is the use of smart materials with self-healing capabilities. Self-healing materials possess the remarkable ability to recover and restore their functionality through reversible chemical bonds [3], [7], [8]. Consequently, soft robots with self-healing capabilities have immense potential to recover their functionality after the healing process [1], [7], [8], [9], [10], [11].

For relatively small-scale damages such as punctures [12], [13], scratches [1], [14], and cuts [8], [9], [10] in self-healing soft robots, the elastomeric properties of soft materials naturally

reconnect the cut surfaces, making recovery easy. However, for large-scale damages such as being split in half, material removal, and deep lengthwise cuts, as shown in Fig. 1, naturally rejoining the cut surfaces is difficult. When the robot has been split in half, a common method is to manually compress the two cut surfaces back together to achieve recovery [9], [13], [14], [15]. A recovery method for closing cut surfaces without manual assistance involved applying magnetic driving force using a permanent magnet [16]. However, this method cannot be performed at room temperature and must be done in an oven, which requires a substantial amount of space. A fish-shaped robot that was split in half can be magnetically closed and repaired at room temperature [17]. However, a larger difference in size between the two damaged pieces can cause lower healing efficiency. Another self-healing soft robot embedded with shape memory alloy (SMA) wires can repair itself when split in half by contracting the SMA wires [18]. This robot can autonomously generate heat to actuate the SMA wires, allowing it to close the cut in the center without external aids. However, because of the low contraction ratio of the SMA wires, the distance between the two cut surfaces should not exceed 2 mm, and this robot cannot recover from material removal or deep lengthwise cuts. To expand the practical applications of soft robots, it is essential that they are developed in such a way that they can autonomously
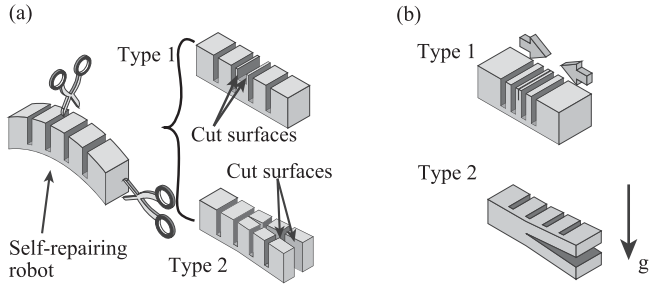
Fig. 2. (a) Damage types. Type 1: Material removal. Type 2: Deep lengthwise cuts. (b) Type 1 damage can be repaired by compression. Type 2 damage can be repaired by gravity.
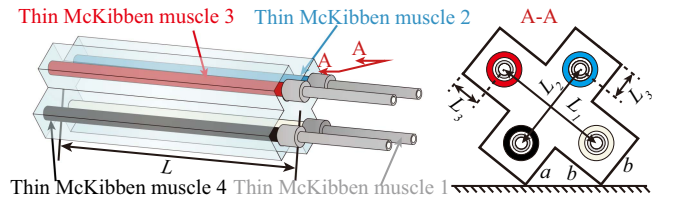

Fig. 3. Prototype of the novel self-repairing soft robot: CAD design and cross-section. Here, $b + 2a = L_2 + 2 \times L_3$ and $3b = L_1 + 2 \times L_3$.
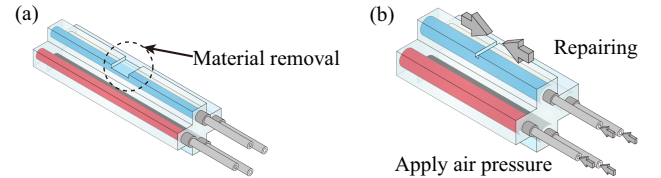

Fig. 4. Schematic of the self-repairing soft robot recovering from material removal. (a) Damage caused by material removal. (b) Apply air pressure to each thin McKibben muscle to close the cut surfaces.
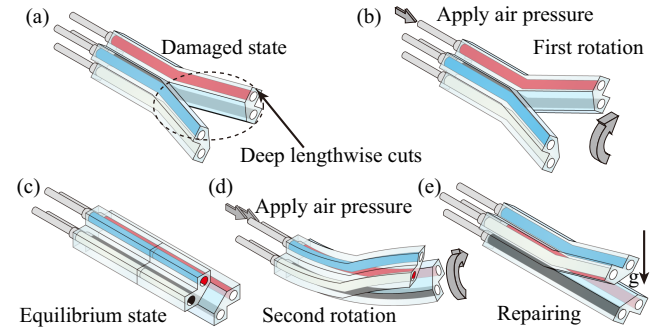

Fig. 5. Recovery of the self-repairing soft robot from deep lengthwise cuts. Although the cut surfaces are much closer, they have been enlarged for visualization purposes. The self-repair process involves the following steps: (a) Determining the damage caused by deep lengthwise cuts. (b) Muscle 3 is pressurized with air, causing the first rotation. (c) Air pressure is removed to reach the equilibrium state. (d) Muscles 2 and 3 are pressurized with air, causing the second rotation. (e) Air pressure is removed to reach the repair state. Finally, the robot's weight causes the crack surfaces to contact each other and be repaired.

heal not only small damages but also more severe damages. One promising method is the use of pneumatic artificial muscles, which have high contraction ratio and ease of operation and control [19]. Our group has previously developed thin McKibben muscles that present unique characteristics; owing to their narrow diameter, they remain flexible even when pressure is applied [5], [20], [21], [22], [23].

In this study, a soft robot capable of repairing material removal and recovering from deep lengthwise cuts without external intervention is proposed. The robot comprises commercially available self-healing materials and thin McKibben muscles with cut-resistant properties. To the best of our knowledge, no previous studies have achieved recovery from material removal or deep lengthwise cuts without external intervention. Bending and crawling locomotion tests were performed to evaluate the self-repairing characteristics.

The remainder of this paper is organized as follows. Section II presents the concept of our novel self-repairing soft robot, along with a mathematical model. Section III describes the fabrication process and setup of the locomotion control system for the self-repairing soft robot. Section IV demonstrates the self-repairing characteristics of the robot after recovery from material removal and deep lengthwise cuts. Conclusions and future works are presented in Section V.

II. DESIGN OF THE SELF-REPAIRING SOFT ROBOT

A. Concept for Self-Repair Damages

As illustrated in Fig. 2, this study proposes closing methods for two specific damages: material removal and deep lengthwise cuts. For material removal, as shown in Fig. 2 (Type 1), contraction is proposed to close the cut surfaces. For the deep lengthwise cuts shown in Fig. 2 (Type 2), the robot's own weight was relied upon to close the cut surfaces.

Based on the self-repair method for these two types of damage, a self-repairing soft robot (shown in Fig. 3) is proposed. It comprises four thin McKibben muscles embedded within self-healing materials in a specific order. The thin McKibben muscle (SM40, s-muscle Co., Ltd) comprises an outer fiber sleeve and an internal silicone rubber tube [21]. The outer sleeve is made of Vectran, a material with cut-resistant properties, ensuring the robot will not split in half. The self-healing material

(WIZARD GEL, Yoshiro) is a commercial product that can be easily produced by mixing the main and hardening agents. After closing the cut surfaces, the healing process is initiated, which involves recombining the host and guest gels [24], [25], [26] at a microscopic level, allowing for macroscopic self-healing. The self-healing material has a hardness of 40 point (CSC2 type) and can be stretched up to 10 times its original length. It exhibits excellent mechanical properties with a tensile strength of 0.24 MPa. Additionally, it only requires contact with the crack surfaces after damage, without needing external triggers, and achieves self-healing within 24 h at room temperature.

To repair material removal, air pressure is applied to all thin McKibben muscles, as shown in Fig. 4, leveraging the high contraction rate to close the cut surfaces. For recovery from deep lengthwise cuts, pressure is first applied to thin McKibben muscle 3, as shown in Fig. 5(b), causing the corresponding part
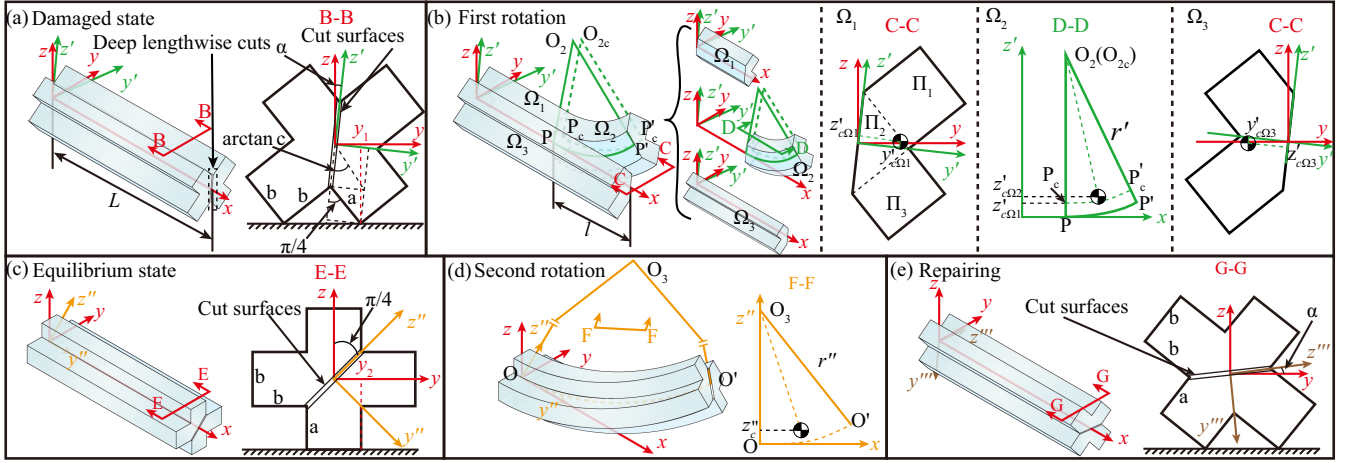
Fig. 6. Analytical model of the self-repairing soft robot recovering from deep lengthwise cuts. (a) Damaged state, dimensional parameters of the robot (body length of the robot L, cut length l), and its critical point for the first rotation (y_1). (b) First rotation: The robot is divided into three parts (Ω_1, Ω_2, and Ω_3). The centers of gravity of the three parts are calculated to determine the overall center of gravity. The first rotation occurs when the entire center of gravity position exceeds the critical point (y_1). (c) Equilibrium state: Critical point for the second rotation (y_2). (d) Second rotation: Calculating the center of gravity of the robot, the second rotation occurring when it exceeds the critical point (y_2). (e) Begin self-repair.

to lift. Consequently, the center of gravity of the robot shifts, achieving the first rotation and reaching an equilibrium state, as shown in Fig. 5(c). Next, pressure is applied to the thin McKibben muscles 2 and 3, as shown in Fig. 5(d), which bends the robot and changes its center of gravity. This results in a second rotation that allows the robot to begin repairing itself, as shown in Fig. 5(e), thereby helping the cut surfaces to connect under their own weight. A mathematical analysis of this process is presented in Section II-B.

B. Mathematical Modeling of the Self-Repairing Soft Robot for Repairing Deep Lengthwise Cuts

The self-repairing soft robot repairs deep lengthwise cuts using the method shown in Fig. 5. The influence of the parameters of the robot on achieving the first and second rotations was determined using mathematical calculations. Before the calculations, the following assumptions were made: i) density for the robot's material is constant, ii) weight of the thin McKibben muscles on the robot is ignored, iii) the cut surfaces are assumed to be infinitely close. Additionally, two variables are defined as follows:

$$c = \frac{a}{b}, \alpha = \frac{\pi}{4} - \arctan\frac{a}{b} \qquad (1)$$

where a is the length of the short side and b is the length of the long side.

As shown in Fig. 6(a), the xyz coordinate system with its origin at the center was established, and for ease of calculation, this xyz coordinate system was rotated clockwise by α rad about the x-axis, creating a new $xy'z'$ coordinate system. The robot's center of gravity must exceed the critical point at the y-coordinate to achieve the first rotation; this critical value y_1 in

the xyz coordinate system can be computed as:

$$y_1 = \frac{\sqrt{2}}{2}a\cos\alpha - \frac{\sqrt{2}}{2}a\left(1 + \frac{1}{c}\right)\sin\alpha \qquad (2)$$

The conditions for achieving the first rotation are shown in Fig. 6(b). The entire robot is divided into three parts, denoted as Ω_1, Ω_2, and Ω_3, and their centers of gravity are calculated in the $xy'z'$ coordinate system. Afterward, the position of the center of gravity of the entire robot is derived in the xyz coordinate system. It is important to note that this model rotates about the x-axis; therefore, we only need to calculate the parameters y_c' and z_c' in the $xy'z'$ coordinate system as follows:

$$y_c' = \frac{\sum_{i=1}^{3} y_{c\Omega_i}' V_{\Omega_i}}{\sum_{i=1}^{3} V_{\Omega_i}}, \; z_c' = \frac{\sum_{i=1}^{3} z_{c\Omega_i}' V_{\Omega_i}}{\sum_{i=1}^{3} V_{\Omega_i}} \qquad (3)$$

where $y_{c\Omega_i}'$ and $z_{c\Omega_i}'$ are the coordinates of the center of gravity of part i in the $xy'z'$ coordinate system, and V_{Ω_i} is the volume of part i. As shown in Fig. 6(b), it is assumed that Ω_1 remains in its initial state and that the center of gravity has the same $y_{c\Omega_1}'$ and $z_{c\Omega_1}'$ for each cross-section, which can be obtained by dividing one cross-section into three parts: Π_1, Π_2, and Π_3, and by calculating the center of gravity for each part individually:

$$\begin{cases} y_{c\Omega_1}' = \frac{a\sqrt{a^2+b^2}\cos\alpha + \frac{7\sqrt{2}}{6}b^2}{2a+3b} \\ z_{c\Omega_1}' = \frac{\sqrt{2}b^2 - a\sqrt{a^2+b^2}\cos\alpha}{2a+3b} \end{cases} \qquad (4)$$

The Ω_2, part of the robot is assumed to move within the xz' plane. The arc length PP' is equal to the cut length l, and the center of gravity of each section is on the arc P_cP_c'. Thus, $y_{c\Omega_2}'$ and $z_{c\Omega_2}'$ can be calculated as:

$$y_{c\Omega_2}' = y_{c\Omega_1}', \; z_{c\Omega_2}' = r' - \frac{r'\left(r' - z_{c\Omega_1}'\right)}{l}\sin\frac{l}{r'} \qquad (5)$$

where r' is the radius of curvature of arc PP', which depends on the applied air pressure. For Ω_3, the values of $y_{c\Omega_3}'$ and $z_{c\Omega_3}'$

can be derived based on the symmetry of Ω_1.

$$y'_{c\Omega_3} = -y'_{c\Omega_1}, \ z'_{c\Omega_3} = -z'_{c\Omega_1} \quad (6)$$

According to the geometric relations shown in Fig. 6(a), V_{Ω_3} and the relations between V_{Ω_1}, V_{Ω_2} and V_{Ω_3} can be derived as follows:

$$V_{\Omega_3} = \frac{1}{2}\left(2a + 3b\right) bL, \ V_{\Omega_1} = \frac{L - l}{L} V_{\Omega_3}, \ V_{\Omega_2} = \frac{l}{L} V_{\Omega_3} \quad (7)$$

where L is the body length of the robot, and the robot's volume remains unchanged. From this, the condition for achieving the first rotation is determined to be

$$y'_c \cos\alpha + z'_c \sin\alpha > y_1 \quad (8)$$

By substituting (2)–(7) into (8), the condition for achieving the first rotation determined by the dimensional parameters of the robot can be derived. Note that $y'_c = 0$ based on symmetry.

$$\frac{l}{L}\left[\frac{r'}{a} - \frac{\frac{\sqrt{2}}{c} - \sqrt{c^2 + 1}\cos\alpha}{2c + 3}\right] \times \left(1 - \frac{r'}{l}\sin\frac{l}{r'}\right)$$
$$- \frac{\sqrt{2}\left(2c^2 + c - 1\right)}{c\left(1 - c\right)} > 0 \quad (9)$$

As shown in Fig. 6(c), the critical value y_2 of the center of gravity of the robot in the xyz coordinate system can be determined to achieve the second rotation.

$$y_2 = \frac{1}{2}b \quad (10)$$

For ease of calculation, the xyz coordinate system is rotated clockwise by $\pi/4$ rad about the x-axis, creating the $xy''z''$ coordinate system. Assuming the robot moves within the xy'' plane after being actuated, the center of gravity of each cross-section is located on the arc OO'. The position of the center of gravity (y''_c, z''_c) in the $xy''z''$ coordinate system under the state of Fig. 6(d) is given by:

$$y''_c = 0, \ z''_c = r''\left(1 - \frac{r''}{L}\sin\frac{L}{r''}\right) \quad (11)$$

where r'' is the radius of curvature of arc OO', which depends on the applied air pressure. The condition for achieving the second rotation is given by:

$$y''_c \cos\frac{\pi}{4} + z''_c \sin\frac{\pi}{4} > y_2 \quad (12)$$

By substituting the relations in (10) and (11) into (12), the condition for achieving the second rotation determined by the dimensional parameters of the robot can be derived.

$$r''\left(1 - \frac{r''}{L}\sin\frac{L}{r''}\right) - \frac{\sqrt{2}}{2}b > 0 \quad (13)$$

According to the analysis of the repair process shown in Fig. 6, the robot will rotate $2\arctan c$ rad and will complete the repair with the assistance of its own weight. Equation (9) shows that if $c \leq 0.5$, the robot cannot maintain its initial state and will undergo the first rotation without actuation. By contrast, if $c = 1$, the robot is a planar symmetrical structure, and it cannot complete the first rotation under any conditions. According to
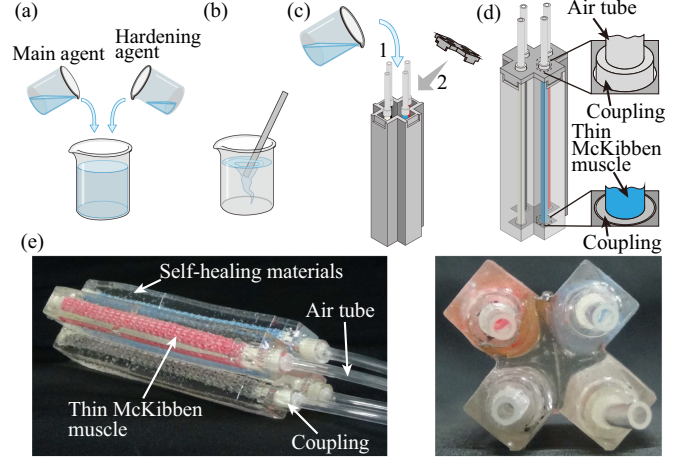

Fig. 7. Fabrication process of the self-repairing soft robot. (a) Mix the main agent and hardening agent. (b) Stir thoroughly to blend the agents. (c) Pour the mixture into the mold. (d) Wait for solidification. (e) The photograph of the self-repairing soft robot.

TABLE I
DIMENSIONS OF THE SELF-REPAIRING SOFT ROBOT

L [mm]	L_1 [mm]	L_2 [mm]	L_3 [mm]	a [mm]	b [mm]
100	20	16	5	8	10

(13), the second rotation can more easily occur after completing the first rotation. Therefore, ensuring that $0.5 < c < 1$ when designing a robot is crucial. The non-planar symmetrical structure of the robot contributes to its rotation.

III. FABRICATION AND CRAWLING EXPERIMENT

A. Fabrication of the Self-Repairing Soft Robot

The fabrication process of the self-repairing soft robot is shown in Fig. 7. First, the main and hardening agents of WIZARD GEL were mixed and stirred in a 100:3 ratio. Then, the mixture was poured into the mold containing the pre-fixed thin McKibben muscles. The mold was left at room temperature for 20–30 min to complete the fabrication process. In this study, the total length of the self-repairing soft robot L was 100 mm, with L_1, L_2, and L_3 (defined in Fig. 3) set to 20, 16, and 5 mm, respectively. Based on the geometric relations of the cross-section shown in Fig. 3, the short side a of the robot is 8 mm, and the long side b is 10 mm. The dimensions of the self-repairing soft robot are summarized in Table I. Based on these dimensions, the variable c (defined in Section II) was determined as 0.8, and α as 0.11 rad.

B. Crawling Experiment

The self-repairing soft robot was controlled using an air pump (SLP-07EED), solenoid valves (KOGANEI025M10F), a stabilized power supply (EX-750L2), and a microcontroller (NUCLEO-F401RE). The detailed actuating mode is shown in Fig. 8.
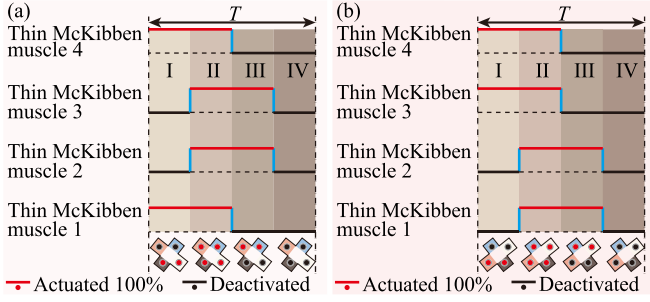
Fig. 8. Actuation modes of the self-repairing soft robot. (a) In virgin state. (b) Recovery from deep lengthwise cuts.
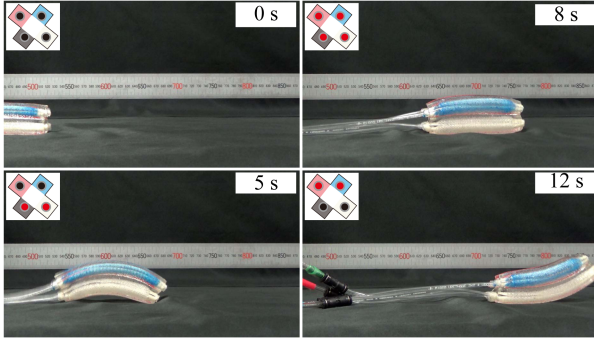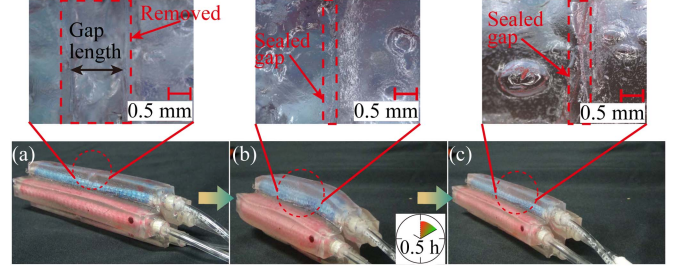

Fig. 10. Process of the self-repairing soft robot recovering from material removal. Here, a digital microscope (VHX-8000 series, KEYENCE) is used to observe the cut surfaces. (a) Damage with a gap length of 1.5 mm. (b) Repairing the damage. (c) Repair accomplished.

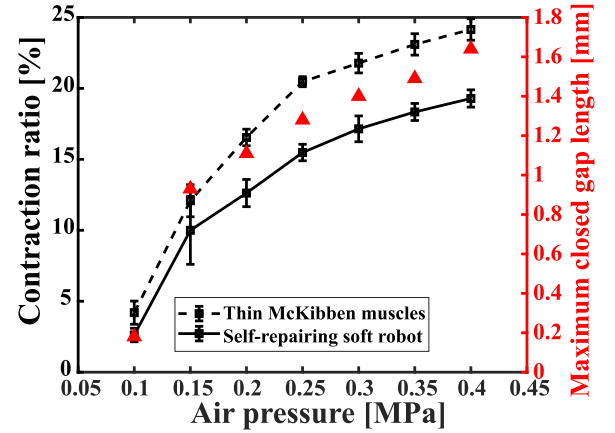Fig. 9. Photograph sequence of the virgin self-repairing soft robot crawling on the textured surface.

Fig. 11. The relationship between applied air pressure and contraction ratio in thin McKibben muscles (black dashed line) and the self-repairing soft robot (black solid line), and the maximum gap length (red triangles) that can be repaired under different air pressure.

In Fig. 8(a), the actuation mode of the robot in its virgin state is presented. It comprises four phases, each with a response time of 0.2 s. The crawling cycle T is 0.8 s. Fig. 8(b) shows the actuation mode of the robot after repairing damage from deep lengthwise cuts. It also has four phases, each with a 0.2 s response time. The crawling cycle T is 0.8 s. The actuation mode differs from its virgin state due to the rotation for damage repair, yet the actuation methods remain the same in both states.

When a pressure of 0.4 MPa is applied to the robot in the virgin state, it can crawl 14 mm within one crawling cycle (14% of its body length). On the textured surface, it can crawl forward at an average speed of 17.3 mm/s, as shown in the photograph sequence in Fig. 9.

IV. SELF-REPAIRING CHARACTERISTICS

A. Self-Repair After Material Removal

Fig. 10 shows a section of the material removed from the self-repairing soft robot in the crosswise direction of the thin McKibben muscle. The width of the removed material is consistent with b in Fig. 3. The depth is limited by L_3 in Fig. 3. The length parallel to the muscle direction is referred to as the gap length. The robot can repair itself following the method shown in Fig. 4. The experimental results indicate that under 0.4 MPa air pressure, material removal of 1.5 mm gap length could be closed. After maintaining this state for 30 min, successful repair was confirmed. No bending was observed

due to the removal of the material after the robot was deactivated. This indicates that the robot can self-repair from material removal.

As shown in Fig. 11, when 0.4 MPa air pressure was applied to the robot, the contraction ratio of the virgin robot was 19%. The maximum gap length it could successfully close was 1.64 mm. This is because only the contraction of muscles near the gap surfaces contributes to their closure. Moreover, the maximum closed gap length varies with air pressure. In the case of material removal, the maximum closed gap length is considered a crucial indicator of repair performance. Therefore, it is necessary to determine the maximum closed gap length that can be repaired under different air pressures. For this purpose, we experimented to measure the maximum closed gap length at different pressures. To do this, we removed a section of the robot and repeated the repair process three times at each specific pressure value. The sealed gap was re-opened between each repair process. The results of the experiment are shown in Fig. 11.

As shown in Fig. 12(a), a part of the robot with a width of 10 mm, depth of 2 mm, and gap length of 1.64 mm was removed. The robot's locomotion performance was tested under the damaged and repaired states. The actuation mode shown in Fig. 8(a) was used for both states. In the damaged state shown
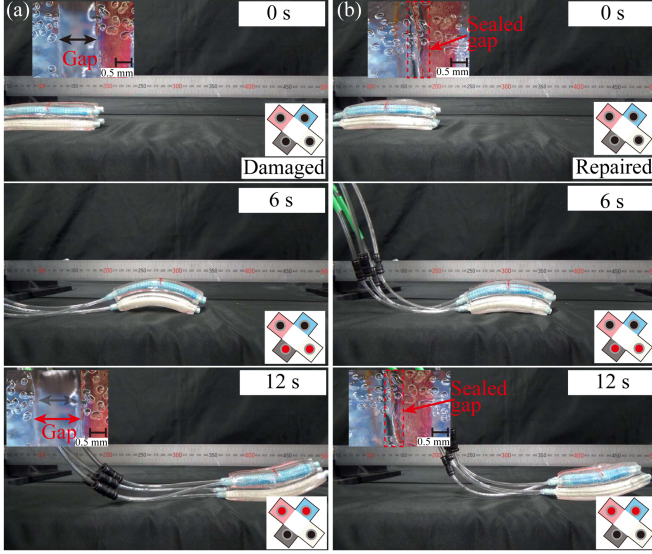
Fig. 12. Photograph sequence of the self-repairing soft robot crawling on a textured surface after material removal and repair. (a) Material removal with a gap length of 1.64 mm. (b) Robot after repair.

in Fig. 12(a), the robot could crawl forward as in its virgin state. Similarly, in the repaired state, it could also crawl forward, as shown in Fig. 12(b). The crawling speeds in two states were 16.4 mm/s and 16.3 mm/s, respectively, which were close to the robot's virgin state speed. This indicates that material removal did not significantly affect the robot's locomotion performance. As shown in Fig. 12(a), the locomotion test in the damaged state started with a gap length of 1.64 mm, which enlarged to 2.51 mm after a period of actuation. The locomotion performance test in the repaired state shown in Fig. 12(b) shows that the cut surfaces could maintain closure before and after actuation.

B. Self-Repair After Deep Lengthwise Cuts

Three self-repairing soft robots were subjected to deep lengthwise cuts with cut lengths of 25, 50, and 75 mm, respectively, shown in Fig. 13. The robots were able to repair themselves by following the method outlined in Section II-A. The experimental results indicate that the robots could complete a two-process rotation under an applied pressure of 0.4 MPa, recovering the cut surfaces by bringing them into contact. After waiting 24 h at room temperature, the recovery was confirmed. This shows that the robot can self-repair from deep lengthwise cuts.

A bending experiment was conducted to demonstrate the feasibility of the first rotation in Fig. 14(a). Based on the mathematical model of the first rotation proposed in Section II-B, Ω_2 moves only in the xz' plane after actuation. However, as indicated by the experiment shown in Fig. 13, Ω_2 tended to move along the y'-axis after actuation. To address this, we improved the model by introducing a correction K_p in the y-coordinate for Ω_2. The function for determining the first rotation is defined

as:

$$f\left(r'\right) = \frac{l}{L}\left[\frac{r'}{a} - \frac{\frac{\sqrt{2}}{c} - \sqrt{c^2 + 1}\cos\alpha}{2c + 3}\right]$$
$$\times \left(1 - \frac{r'}{l}\sin\frac{l}{r'}\right) - \frac{\sqrt{2}\left(2c^2 + c - 1\right)}{c\left(1 - c\right)} + K_p \quad (14)$$

where the radius of curvature in the first rotation (r') and dimensions of the robot (l, L, a, c, and α) are consistent with the definition in Section II-B. The bending experiments shown in Fig. 14(a) were conducted under three different cut lengths (25, 50, and 75 mm) to obtain the mean and standard deviation of the K_p values under different air pressures, shown in Fig. 14(b). As an example, for a robot with a cut length of 50 mm, the conditions for achieving the first rotation can be obtained by substituting the robot's dimensions shown in Table I and the standard deviation of K_p at 0.15, 0.2, 0.3, and 0.4 MPa from Fig. 14(b) into (14), as shown in Fig. 14(c). The robot with a cut length of 50 mm required a pressure of 0.3 MPa or more to complete the first rotation. The pressure needed to achieve the first rotation for robots with cut lengths of 25 and 75 mm can be similarly determined.

A bending experiment for the second rotation was conducted, as shown in Fig. 15(a). The function for determining the second rotation is defined as:

$$f\left(r''\right) = r''\left(1 - \frac{r''}{L}\sin\frac{L}{r''}\right) - \frac{\sqrt{2}}{2}b \quad (15)$$

where the radius of curvature in the second rotation (r'') and dimensions of the robot (L, b) are consistent with the definition in Section II-B. By substituting the values from Table I into (15), the conditions for achieving the second rotation can be derived. As shown in Fig. 15(b), different r'' under different pressures of 0.15, 0.2, 0.3, and 0.4 MPa were measured and compared with (15). The second rotation can be attained when a pressure of 0.2 MPa or greater is applied to the robot. Based on the analysis of the mathematical model described above, the second rotation is achieved under the conditions for achieving the first rotation. This is also consistent with the experimental results shown in Fig. 13.

Through bending experiments shown in Fig. 15(a), we measured the crosswise displacement (d) of the robot in virgin, damaged, and repaired states. The following relation can be derived based on geometric relations:

$$d = r''\left(1 - \cos\frac{L}{r''}\right) \quad (16)$$

The theoretical d under different pressures can be calculated by substituting the r'' values computed at 0.15, 0.2, 0.3, and 0.4 MPa from Fig. 15(b) into (16). The results are presented in Fig. 15(c), along with the experimental values for comparison. The value of d for the robot increased with pressure in all conditions. In the virgin state, the value of d reached a maximum of 54 mm at 0.4 MPa. In the damaged state, the value of d decreased significantly with increasing cut length. The value of d for a cut length of 25 mm was 38 mm at 0.4 MPa. After repair,
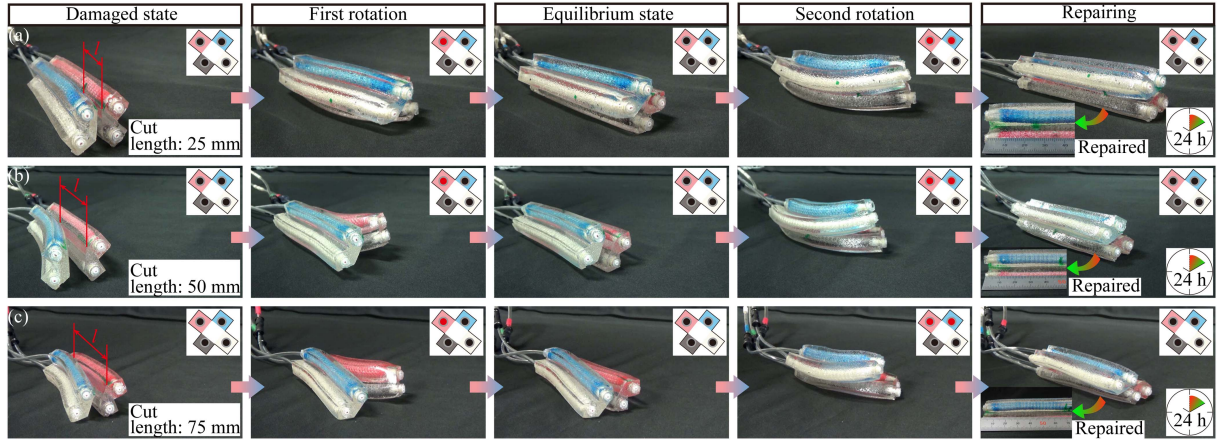
Fig. 13. Photograph sequence of the self-repairing soft robot recovering from deep lengthwise cuts. The cut length is (a) 25 mm, (b) 50 mm, and (c) 75 mm.
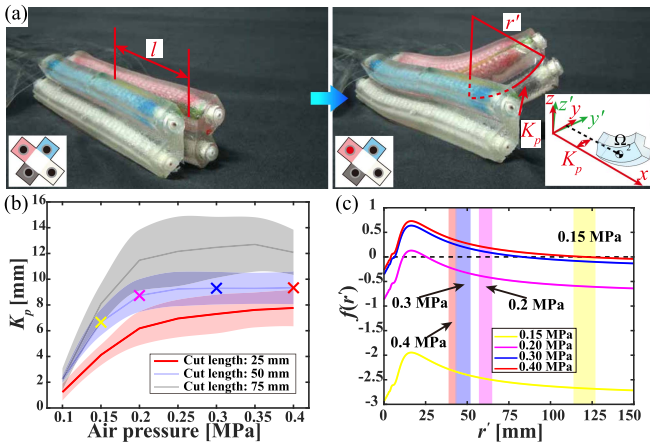

Fig. 14. (a) Bending experiment of the self-repairing soft robot to achieve first rotation. (b) Correction values for different cut lengths under different pressures were applied. (c) Condition for a robot with a cut length of 50 mm to achieve the first rotation. The shaded regions show the experimental values of the radius of curvature (r') under different air pressures.
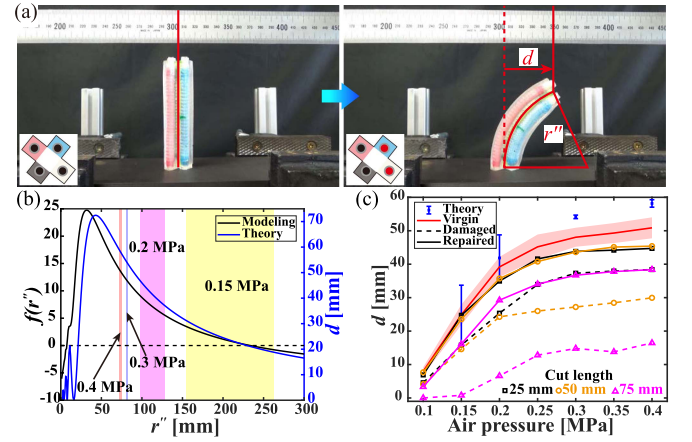

Fig. 15. (a) Bending experiment of the self-repairing soft robot to achieve second rotation. (b) Experimental radius of curvature (r'') was measured under different air pressures. Additionally, the condition required to achieve the second rotation and the theoretical displacement values were determined for different radii of curvature. (c) Displacement under different conditions.

the value of d for cut lengths of 25 mm and 50 mm reached 44 mm and 45 mm, respectively, at 0.4 MPa. By contrast, the value of d for a cut length of 75 mm was 38 mm. This proves that the robot, after deep lengthwise cuts of 25 and 50 mm, has good repair properties.

Ten locomotion tests were conducted for each of the three robots shown in Fig. 13 in both their damaged and repaired states. As shown in Fig. 16(a), in its damaged state, the robot with a cut length of 50 mm cannot crawl forward as it does in its virgin state (see the actuation mode in Fig. 8(a)). This is mainly because the damaged part cannot effectively contribute to the forward crawl upon actuation. The actuation mode for the repaired robot shown in Fig. 16(b) is shown in Fig. 8(b). Comparing the two sequences, it is evident that the robot can crawl forward again as in its virgin state. In particular, after repairing the cut lengths of 25 and 50 mm, the cut surfaces were aligned in most directions, and their crawling speeds reached 13.8 mm/s and 12.1 mm/s, respectively. After repairing a cut
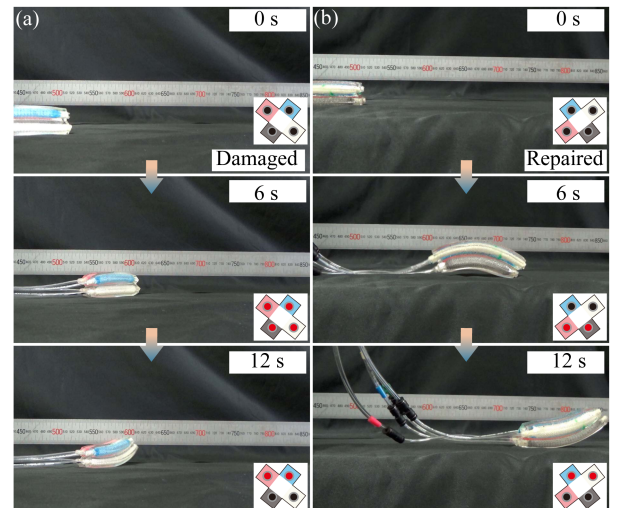

Fig. 16. Photograph sequence of the self-repairing soft robot crawling on a textured surface. (a) Robot with a cut length of 50 mm. (b) Robot after repair.

length of 75 mm, the cut surfaces could not be aligned in most directions, and its crawling speed was reduced to 5.6 mm/s. Therefore, the locomotion performance of a repaired robot is affected by the alignment of its cut surfaces in all directions: fewer parts aligned post-repair results in decreased locomotion performance.

V. Conclusion

This letter investigated the ability of soft robots to repair material removal and deep lengthwise cuts self-repair. A novel self-repairing soft robot actuated by thin McKibben muscles was proposed. In the material removal, the robot closed the gap in cut surfaces with a maximum contraction ratio of up to 19%. The experimental results showed that the robot recovered from a maximum gap length of 1.64 mm when maintaining an air pressure of 0.4 MPa for 30 min. To repair deep lengthwise cuts, the robot can rotate in $2 \arctan c$ rad such that the cut surfaces are closed under the robot's own weight. For lengthwise cuts of 25, 50, and 75 mm, recovery was achieved following a two-process rotation and allowing to bound for 24 h. For lengthwise cuts of 25 and 50 mm, the changes in bending ability after repair were small compared with those in the virgin state, considering the displacement during the damaged state. Correspondingly, the crawling speed in the virgin state reached 17.3 mm/s, whereas after repair, it was 13.8 mm/s. Thus, the proposed self-repairing soft robot allows for material removal and deep lengthwise cuts to be repaired without external intervention.

In the future, we aim to enhance the reliability of robots following repairs involving material removal and deep lengthwise cuts. Various factors, such as surface roughness, weight, and alignment, need to be explicitly considered in the robot's post-repair performance. Experiments should be performed to investigate the types of damages the robot can self-repair, such as cuts made at different angles and damages to the thin McKibben muscles. This may involve considering new structures or replacing the muscle's inner silicone tubes with self-healing materials. Building upon the findings of this study, we hope to achieve an autonomously self-repair robot. This involves incorporating sensing devices such as E-skin and optomechanical sensors, to detect damage types and designing a feedback control system. Autonomous self-repair robots are expected to be extrapolated to other systems for a wide range of applications.

References

[1] S. Terryn, J. Brancart, D. Lefeber, G. V. Assche, and B. Vanderborght, "Self-healing soft pneumatic robots," *Sci. Robot.*, vol. 2, no. 9, 2017, Art. no. eaan4268.

[2] A. López-Díaz, A. Braic, F. Ramos, I. Payo, E. Vázquez, and A. S. Vázquez, "Hydrogel-based soft pneumatic bending actuator with self-healing and proprioception capabilities," in *Proc. IEEE 5th Int. Conf. Soft Robot.*, 2022, pp. 370–375.

[3] E. Roels et al., "Processing of self-healing polymers for soft robotics," *Adv. Mater.*, vol. 34, no. 1, 2022, Art. no. 2104798.

[4] M. Calisti, G. Picardi, and C. Laschi, "Fundamentals of soft robot locomotion," *J. Roy. Soc. Interface*, vol. 14, no. 130, 2017, Art. no. 20170101.

[5] R. Kobayashi, H. Nabae, G. Endo, and K. Suzumori, "Soft tensegrity robot driven by thin artificial muscles for the exploration of unknown spatial configurations," *IEEE Robot. Automat. Lett.*, vol. 7, no. 2, pp. 5349–5356, Apr. 2022.

[6] Z. Zhang, X. Wang, S. Wang, D. Meng, and B. Liang, "Design and modeling of a parallel-pipe-crawling pneumatic soft robot," *IEEE Access*, vol. 7, pp. 134301–134317, 2019.

[7] A. Naranjo et al., "Autonomous self-healing hydrogel with anti-drying properties and applications in soft robotics," *Appl. Mater. Today*, vol. 21, 2020, Art. no. 100806.

[8] F. Jiang, Z. Zhang, X. Wang, G. Cheng, Z. Zhang, and J. Ding, "Pneumatically actuated self-healing bionic crawling soft robot," *J. Intell. Robot. Syst.*, vol. 100, pp. 445–454, 2020.

[9] S. Terryn, J. Brancart, E. Roels, G. V. Assche, and B. Vanderborght, "Room temperature self-healing in soft pneumatic robotics: Autonomous self-healing in a diels-alder polymer network," *IEEE Robot. Automat. Mag.*, vol. 27, no. 4, pp. 44–55, Dec. 2020.

[10] H. Bai, Y. S. Kim, and R. F. Shepherd, "Autonomous self-healing optical sensors for damage intelligent soft-bodied systems," *Sci. Adv.*, vol. 8, no. 49, 2022, Art. no. eabq2104.

[11] W. Tang et al., "Self-protection soft fluidic robots with rapid large-area self-healing capabilities," *Nature Commun.*, vol. 14, no. 1, 2023, Art. no. 6430.

[12] R. F. Shepherd, A. A. Stokes, R. Nunes, and G. M. Whitesides, "Soft machines that are resistant to puncture and that self seal," *Adv. Mater.*, vol. 25, pp. 6709–6713, 2013.

[13] S. Terryn, E. Roels, J. Brancart, G. V. Assche, and B. Vanderborght, "Self-healing and high interfacial strength in multi-material soft pneumatic robots via reversible Diels–Alder bonds," *Actuators*, vol. 9, no. 2, 2020, Art. no. 34.

[14] E. Roels, S. Terryn, J. Brancart, G. V. Assche, and B. Vanderborght, "A multi-material self-healing soft gripper," in *Proc. 2nd IEEE Int. Conf. Soft Robot.*, 2019, pp. 316–321.

[15] H.-Q. Wang, Z.-Y. Huang, D.-W. Yue, F.-Z. Wang, and C.-H. Li, "A variable-stiffness and healable pneumatic actuator," *Mater. Horiz.*, vol. 10, no. 3, pp. 908–917, 2023.

[16] K. Cerdan, G. V. Assche, P. V. Puyvelde, and J. Brancart, "A novel approach for the closure of large damage in self-healing elastomers using magnetic particles," *Polymer*, vol. 204, 2020, Art. no. 122819.

[17] E. Karshalev et al., "Swimmers heal on the move following catastrophic damage," *Nano Lett.*, vol. 21, no. 5, pp. 2240–2247, 2021.

[18] S. K. Tabrizian et al., "Assisted damage closure and healing in soft robots by shape memory alloy wires," *Sci. Rep.*, vol. 13, no. 1, 2023, Art. no. 8820.

[19] G. Andrikopoulos, G. Nikolakopoulos, and S. Manesis, "A survey on applications of pneumatic artificial muscles," in *Proc. 19th Mediterranean Conf. Control Automat.*, 2011, pp. 1439–1446.

[20] S. Wakimoto, K. Suzumori, and J. Takeda, "Flexible artificial muscle by bundle of McKibben fiber actuators," in *Proc. IEEE/ASME Int. Conf. Adv. Intell. Mechatron.*, 2011, pp. 457–462.

[21] S. Kurumaya, H. Nabae, G. Endo, and K. Suzumori, "Exoskeleton inflatable robotic arm with thin McKibben muscle," in *Proc. IEEE Int. Conf. Soft Robot.*, 2018, pp. 120–125.

[22] S. Koizumi, S. Kurumaya, H. Nabae, G. Endo, and K. Suzumori, "Recurrent braiding of thin McKibben muscles to overcome their limitation of contraction," *Soft Robot.*, vol. 7, no. 2, pp. 251–258, 2020.

[23] S. Tanaka, H. Nabae, and K. Suzumori, "Back-stretchable McKibben muscles: Expanding the range of antagonistic muscle driven joints," *IEEE Robot. Automat. Lett.*, vol. 8, no. 9, pp. 5331–5337, Sep. 2023.

[24] A. Harada, R. Kobayashi, Y. Takashima, A. Hashidzume, and H. Yamaguchi, "Macroscopic self-assembly through molecular recognition," *Nature Chem.*, vol. 3, no. 1, pp. 34–37, 2011.

[25] T. Kakuta, Y. Takashima, and A. Harada, "Highly elastic supramolecular hydrogels using host–guest inclusion complexes with cyclodextrins," *Macromolecules*, vol. 46, no. 11, pp. 4575–4579, 2013.

[26] T. Kakuta, Y. Takashima, M. Nakahata, M. Otsubo, H. Yamaguchi, and A. Harada, "Preorganized hydrogel: Self-healing properties of supramolecular hydrogels formed by polymerization of host–guest-monomers that contain cyclodextrins and hydrophobic guest groups," *Adv. Mater.*, vol. 25, no. 20, pp. 2849–2853, 2013.